Atmospheric Research 203 (2018) 175–188

Contents lists available at ScienceDirect

Atmospheric Research

journal homepage: www.elsevier.com/locate/atmosres

Evaluating anemometer drift: A statistical approach to correct biases in wind speed measurement

Cesar Azorin-Molina[a,*], Jesus Asin[b], Tim R. McVicar[c,d], Lorenzo Minola[a], Juan I. Lopez-Moreno[e], Sergio M. Vicente-Serrano[e], Deliang Chen[a]

[a] Regional Climate Group, Department of Earth Sciences, University of Gothenburg, Sweden
[b] Department of Statistical Methods, University of Zaragoza, Zaragoza, Spain
[c] CSIRO Land and Water, Canberra, ACT, Australia
[d] Australian Research Council Centre of Excellence for Climate System Science, University of New South Wales, Sydney, Australia
[e] Instituto Pirenaico de Ecología, Consejo Superior de Investigaciones Científicas (IPE-CSIC), Departamento de Procesos Geoambientales y Cambio Global, Zaragoza, Spain

ARTICLE INFO

Keywords:
Wind speed
Bearing ageing
Intercomparison
Regression models
Stilling phenomenon

ABSTRACT

Recent studies on observed wind variability have revealed a decline (termed "stilling") of near-surface wind speed during the last 30–50 years over many mid-latitude terrestrial regions, particularly in the Northern Hemisphere. The well-known impact of cup anemometer drift (i.e., wear on the bearings) on the observed weakening of wind speed has been mentioned as a potential contributor to the declining trend. However, to date, no research has quantified its contribution to stilling based on measurements, which is most likely due to lack of quantification of the ageing effect. In this study, a 3-year field experiment (2014–2016) with 10-minute paired wind speed measurements from one new and one malfunctioned (i.e., old bearings) SEAC SV5 cup anemometer which has been used by the Spanish Meteorological Agency in automatic weather stations since mid-1980s, was developed for assessing for the first time the role of anemometer drift on wind speed measurement. The results showed a statistical significant impact of anemometer drift on wind speed measurements, with the old anemometer measuring lower wind speeds than the new one. Biases show a marked temporal pattern and clear dependency on wind speed, with both weak and strong winds causing significant biases. This pioneering quantification of biases has allowed us to define two regression models that correct up to 37% of the artificial bias in wind speed due to measurement with an old anemometer.

1. Introduction

Near-surface (i.e. ~10-meter height) wind speed has declined on average −0.140 meter per second per decade ($m\,s^{-1}\,dec^{-1}$) over continental surfaces in the last 30–50 years (McVicar et al., 2012); a phenomenon termed "stilling" for the first time by Roderick et al. (2007). The drivers behind this weakening in observed wind speed have been partly attributed to: (i) changes in land surface friction force because of forest growth, urbanization and other land use changes (Vautard et al., 2010; Bichet et al., 2012; Wever, 2012); (ii) decadal variability of atmospheric circulation (Lu et al., 2007; Azorin-Molina et al., 2014, 2016); (iii) increase of aerosol emissions and greenhouse gas concentrations (Jacobson and Kaufman, 2006; Xu et al., 2006); (iv) decrease of the spatial variance in both atmospheric pressure and air temperature (Kim and Paik, 2015); (v) positive trends in available soil water (Shuttleworth et al., 2009); (vi) astronomical changes (Mazzarella, 2007); and (vii) instrumental issues including technological improvements of wind sensors, maintenance and calibration issues, shifts in measurement sites, and time intervals at which data is stored (Wan et al., 2010; Azorin-Molina et al., 2017a). However, the causes of stilling remains uncertain as all these issues are likely occurring simultaneously with varying spatio-temporal variance. Moreover, some studies have recently claimed that this terrestrial stilling has broken in some regions (Kim and Paik, 2015; Dunn et al., 2016; Azorin-Molina et al., 2017b). Therefore, further research to assess and, particularly, improve the attribution of wind speed trends and cycles is strongly needed.

Among the instrumental artefacts related to the loss of cup anemometer performance, Pindado et al. (2014) pointed out three issues that affect the accuracy of wind speed measurements: (i) wear and tear with the internal anemometer bearings (i.e., degrading its rotor) and, secondarily, the mass addition of dirt to the cups (i.e., changing its aerodynamics); (ii) rotor damage due to severe storms, hail or lightning; and (iii) failure at the opto-electronic output signal system. The first impact

* Corresponding author address: Cesar Azorin-Molina, Department of Earth Sciences, University of Gothenburg, Box 460, 405 30 Gothenburg, Sweden.
E-mail address: cesar.azorin-molina@gu.se (C. Azorin-Molina).

https://doi.org/10.1016/j.atmosres.2017.12.010
Received 27 November 2017; Accepted 20 December 2017
Available online 23 December 2017
0169-8095/

of anemometer drift (i.e., bearings malfunctions) has only been superficially discussed as a possible cause of stilling (Wan et al., 2010; Azorin-Molina et al., 2014), and because of its complexity, to date, no research has attempted to quantify and minimize the contribution of anemometer degradation to the stilling phenomenon. Pindado et al. (2014) noted that the gradual drift of cup anemometers occurred due to instrument ageing and results in a progressive and artificial decrease of measured wind speed over time because of the reduction in the rotational speed. This degradation (i.e., increase of friction) has most impact in weak winds and, consequently, increases the periods of observed calms (Pindado et al., 2014). In theory, National Weather Services apply a maintenance program to periodically inspect and/or recalibrate cup anemometers to ensure accuracy of instruments. However, because of the limited metadata about field calibration of cup anemometers (e.g., frequency of recalibrations, etc.; Azorin-Molina et al., 2014), and even assuming that annual inspections are conducted, as recommended by the World Meteorological Organization (WMO, 2008), anemometer ageing is a concern when analyzing long-term wind speed variability and trends. Therefore, anemometer drift is hypothetically a partial cause of the stilling that deserves to be assessed and corrected. This study fills this knowledge gap.

The assessment of cup anemometer working health is challenging (Siegel and Lee, 2011) as damaged or used instruments can produce reasonable wind speed measurements (Pindado et al., 2014). Previous studies assessing the behavior of anemometers in measuring wind speed have focused on: (i) the number of cups and arm length (Marvin, 1932); (ii) the aerodynamic of cups (Marvin, 1934); (iii) the frequency system to record data (Charnock and Pierce, 1959); (iv) the over-estimating errors in fluctuating winds (Deacon, 1951); (v) the impact of environmental-climatic conditions (Kimura et al., 2001); (vi) the loss of performance of wind speed sensors and the deviations of calibration coefficients (Pindado et al., 2012); (vii) anemometer condition diagnosis problem (Sun et al., 2012); (viii) the study of the geometry of cups to improve the uniformity of anemometer rotation and reduce degradation due to ageing (Pindado et al., 2014); and (ix) the errors of cup anemometer rotational speed (Martinez et al., 2016), among other instrumental issues. Many recent anemometer performance studies were performed to assess the impact of measurement accuracy on the wind energy sector (i.e., wind turbine power performance; Pindado et al., 2014). However, interest in advancing a comprehensive attribution of the stilling phenomenon also has other scientific, socioeconomic and environmental impacts (Azorin-Molina et al., 2017a), particularly because the impact of wind speed on atmospheric evaporative demand (e.g., McVicar et al., 2012; Limjirakan and Limsakul, 2012) and air pollutant concentrations (e.g., Tong et al., 2017), among others.

The aims of this study are to: (i) assess divergences in measuring wind speed due to the cup anemometer drift (i.e., wear on the bearings); and (ii) define statistical approaches to correct biases in wind speed measurement due to the artificial decline signal produced by anemometer-bearing ageing. Our ultimate goal is to improve the long-term assessment of wind speed trends. The paper is structured as follows: Section 2 describes the experimental design and methodology; Section 3 deals with the results of the intercomparison addressing objective (i) above; Section 4 proposes and assesses two statistical approaches to minimize errors addressing objective (ii); and Sections 5 and 6 discusses and summarizes the findings of this research, respectively.

2. Experimental design, paired data and statistical analyses

2.1. Cup anemometers and experiment setup

The first hemispherical cup anemometer was invented by John Thomas Romney Robinson in 1846 (Robinson, 1847), and consisted of four cups-arms instead of three that Patterson (1926) designed some decades later to improve its response and aerodynamics. The standardized three-cup anemometer is still the most widely used wind measuring instrument for the wind energy sector (i.e., production forecast and wind mill performance control; Pindado et al., 2015) and in meteorological applications (WMO, 2008). Due to its simplicity, it is inexpensive when compared to sonic or propeller devices, shows an accurate linear response in the usual range of wind speed (i.e., 4–16 m s^{-1}) (Kristensen, 1998), and it can operate under extreme weather conditions (Makkonen et al., 2001). Therefore, almost all long-term wind speed time series have been measured by cup anemometers (McVicar et al., 2012) and assessing the drift due to the wear and tear on the internal bearings of three-cup anemometers is of key importance.

Table 1
Technical specifications of the SEAC SV5 cup anemometer used in this study.

General and electrical features	Specifications
Measuring system	Opto-electronic pulse generator (20 pulses/meter)
Measurement range	0.0 to 65.0 m s^{-1}
Threshold sensibility	0.2 m s^{-1}
Resolution	0.05 m s^{-1}
Accuracy	± 2.0%
Transducer type	LED phototransistor
Power supply	5 to 12VDC
Power consumption	300 mW

Dimensions	Specifications
Weight	0.30 kg
Height (cup wheel included)	235 mm
Case diameter	55 mm
Cup wheel diameter	120 mm
Material	Injected aluminium with anticorrosive paint

The cup anemometer chosen for this intercomparison study was the 3-cup *Sociedad Española de Aplicaciones Cibernéticas SA* (SEAC; http://www.seac.es/; last accessed 1 November 2017) anemometer SV5. This SEAC SV5 anemometer has been in continual operation in most automatic weather stations (AWS) of the Spanish Meteorological Agency (AEMET) since the mid-1980s (Azorin-Molina et al., 2014). Technical specifications regarding the SEAC SV5 are summarized in Table 1 along with pictures shown in Fig. 1a. For the intercomparison, two SEAC SV5 were used: (i) one new anemometer purchased from SEAC (hereafter 'SEAC-new'); and (ii) one anemometer rescued from an AWS after some years of operation (hereafter 'SEAC-old'). The SEAC-old was delivered to SEAC to replace: (i) the 3-cups and arms; and (ii) the opto-electronic output signal system, with new ones. The used bearings were not subject to any maintenance and/or replacement to assess the impact of anemometer drift on wind speed measurements when compared to SEAC-new; i.e., both anemometers only differ in the age of the bearings. Furthermore, before the paired-anemometer experiment, wind tunnel tests (see Fig. 1b) were performed by SEAC to ensure the optimal performance of the SEAC-new against a reference anemometer, and prove the rotor response of the SEAC-old. Test results in the tunnel estimated that the SEAC-old underestimated wind speed below the threshold of 3 m s^{-1}, whereas it showed an almost linear response to the reference anemometer above 7 m s^{-1}; parallel wind speed data performed in the tunnel tests were not recorded and, therefore, cannot be shown.

The experiment consisted of mounting the two anemometers 9 m above ground-level i.e., almost on top of a 10 m meteorological tower in Villena (Alicante; south-eastern Spain; 38°37′42.41″N and 0°56′05.25″W; 497 m above sea level; and ~50 km from the Mediterranean shore; see Fig. 1c). Both cup anemometers were separated by a distance of 1.5 m, with the horizontal mast oriented from 95° (i.e., where SEAC-old is located) to 275° (i.e., where SEAC-new is placed). The field site is located in a valley within the Prebetic System Mountains (Fig. 2a), representing a cold semi-arid climate (BSk)

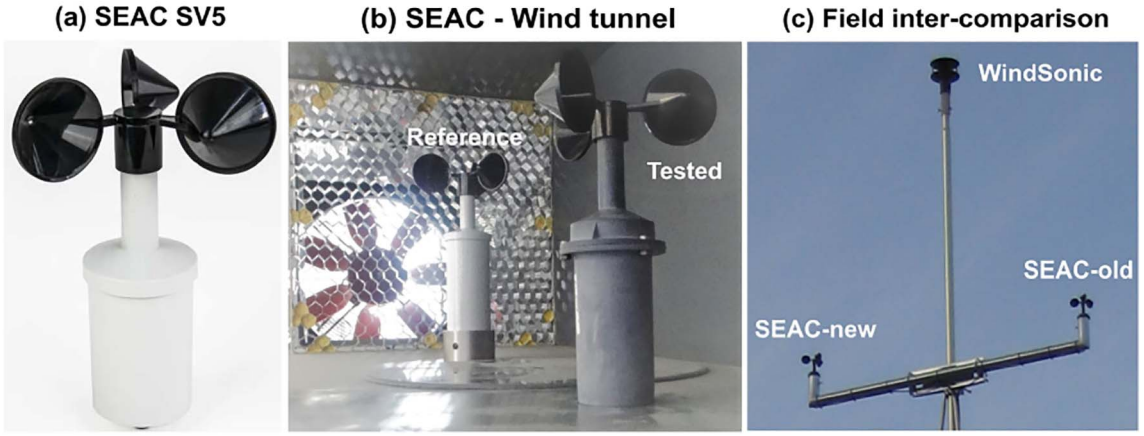

Fig. 1. Part (a) standardized 3-cup SEAC-SV5 anemometer; (b) wind tunnel tests carried out between the reference and tested anemometers; and (c) experimental set-up of both SEAC-new and SEAC-old cup anemometers at the height of 9 m and separated by a distance of 1.5 m in the meteorological tower of Villena (Spain). A windsonic anemometer was already located at 10 m above the ground. (For interpretation of the references to color in this figure legend, the reader is referred to the web version of this article. The same for the rest of colour figures in the manuscript.)

according to the Köppen climate classification. In general, winds are dominated by local wind circulations in spring-summer (i.e., May–October), with distinct sea breezes and coastal low level jets (Kottmeier et al., 2000), and large-scale synoptic winds in autumn-winter (i.e., November–April), (Azorin-Molina et al., 2011); see Section 2.3. Technical issues prevented placing both cup anemometers at the top of the tower, next to and at the same level as the AWS sonic anemometer. Fig. 2b shows an overview of the field site with the meteorological tower along with other weather instruments measuring: wind direction, wind speed, air temperature, relative humidity, air pressure, global solar radiation and precipitation.

2.2. Wind speed paired data

Both cup anemometers were connected to a ZENO® 3200 datalogger (http://www.coastalenvironmental.com/zeno-datalogger.shtml; last accessed 1 November 2017) which monitored the output frequency for each one, and computed and stored mean wind speed (in m s^{-1}) at 10-minute intervals. Table 2 summarizes monthly descriptive statistics about the sample and anemometer bias for the 3-year field experimental campaign from 1 Jan 2014 to 31 Dec 2016. For a robust assessment of the anemometer drift, the following irregular paired wind speed data (outliers) were eliminated, due to: (i) ZENO® 3200 datalogger troubles/inconsistency when reading the output frequency of

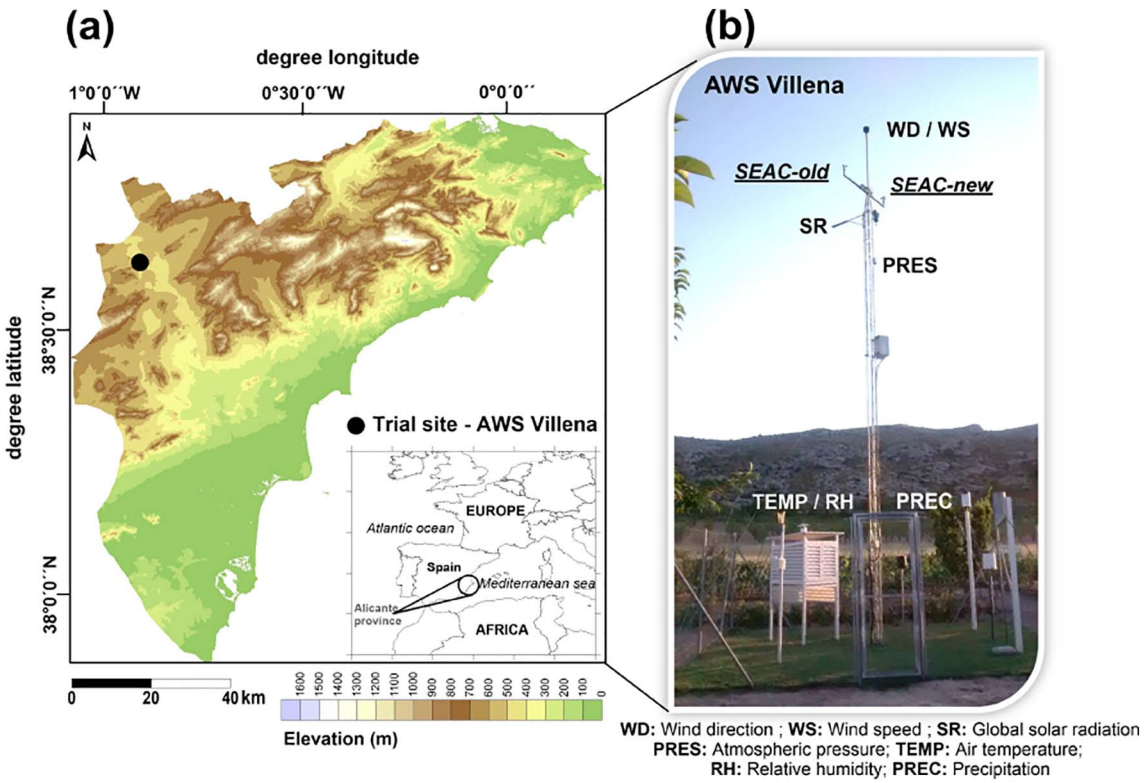

Fig. 2. (a) Terrain map of the Alicante province showing the location of the automatic weather station chosen for the experiment-setup. (b) Picture illustrating the AWS in Villena (Spain), the locations of both SEAC-new and SEAC-old cup anemometers and the other weather instrument available for measuring complementary atmospheric parameters. (For interpretation of the references to color in this figure legend, the reader is referred to the web version of this article. The same for the rest of colour figures in the manuscript.)

Table 2
Descriptive table of the monthly number of paired data (Ndat), number of missing values (NAs), number of differences below (N < 0) or equal (N = 0) to 0 that have been discarded in the analyses, and mean, standard deviation (Sd), 25th (Q1), 50th (Q2), and 75th (Q3) percentiles, and maximum (Max) values of the differences in mean wind speed of SEAC-new minus SEAC-old for the 3-year experiment.

Month	Ndat	NAs	N < 0	N = 0	Mean m s^{-1}	Sd m s^{-1}	Q1 m s^{-1}	Q2 m s^{-1}	Q3 m s^{-1}	Max m s^{-1}
Jan	12607	784	1393	1573	0.24	0.28	0.01	0.21	0.41	2.12
Feb	12222	18	746	529	0.33	0.23	0.21	0.34	0.47	3.81
Mar	13390	2	731	1731	0.29	0.24	0.07	0.31	0.44	1.78
Apr	12956	4	285	1478	0.31	0.23	0.13	0.31	0.45	1.88
May	13384	8	1135	1978	0.25	0.26	0.01	0.22	0.42	1.47
Jun	12956	4	1192	1663	0.24	0.25	0.03	0.21	0.42	1.20
Jul	11931	1461	845	1627	0.25	0.31	0.04	0.21	0.44	1.49
Aug	8914	4476	298	1432	0.28	0.36	0.09	0.26	0.48	1.34
Sep	8624	4336	234	1344	0.32	0.32	0.09	0.32	0.52	2.10
Oct	12812	577	677	2247	0.24	0.24	0.02	0.21	0.38	2.17
Nov	12958	2	1334	2344	0.20	0.24	0.00	0.18	0.34	2.23
Dec	13389	3	2442	3607	0.08	0.22	0.00	0.04	0.22	2.15

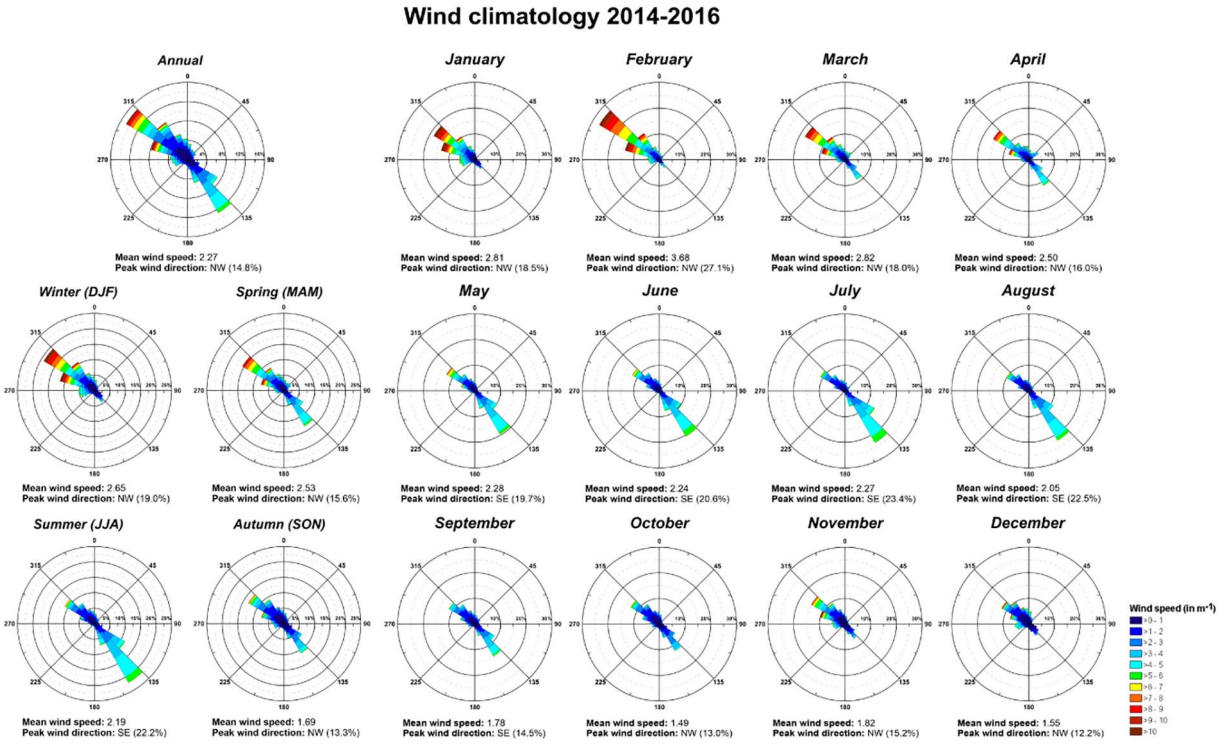

Fig. 3. Annual, seasonal and monthly wind roses in Villena for 2014–2016. (For interpretation of the references to color in this figure legend, the reader is referred to the web version of this article. The same for the rest of colour figures in the manuscript.)

both anemometers; (ii) two severe storms with large hail that damaged cups of the SEAC-new (from 22-Jul till 16-Aug-2015) and both anemometers (from 27-Sep till 04-Oct-2015 – with cups being replaced as outlined below); (iii) sheltering by the tubular mast of the anemometers (i.e., blocking effect to the surrounding air) forced the removal of two narrow wind direction sectors (i.e., from 80° to 110° and 260° to 290°); and (iv) anomalous negative differences between the anemometers, assuming that 10-minute mean wind speeds must be always greater in SEAC-new than SEAC-old (pers. comm. with the technical staff from SEAC). All these criteria for data removal were previously applied in anemometer intercomparisons (e.g., Sun et al., 2012), resulting in negligible change in the overall mean wind speed difference and the assessment. To summarize, quantitative analyses of data shown in this assessment are based on a total of 101,603 paired measurements at 10-minute intervals, after removing 44,540 paired data as NAs (11,675) or ≤ 0 (32,865) values. Moreover, the damaged cups in (ii) above were repaired by SEAC and to ensure the accuracy of SEAC-new throughout the 3-years of field experiment, bearings were maintained and a recalibration applied. Lastly, the sonic anemometer served to quality-control the paired wind speed measurements and plot the wind rose climatology at our field site.

2.3. Wind climatology

Fig. 3 shows the annual, seasonal and monthly wind roses in Villena for 2014–2016. For all time-scales, atmospheric wind circulation is mainly driven by two major patterns, as previously concluded (Azorin-Molina and Martin-Vide, 2007; Azorin-Molina et al., 2011): (i) northwesterly synoptic winds (300°–315°; hereafter NW); and (ii) southeasterly local winds (135°–150°; hereafter SE). Annual wind rose depicts a dominance of NW flows (14.8%) followed by SE winds (12.8%), with a mean wind speed of 2.27 m s^{-1}. Seasonally, synoptic NW flows mainly dominated in winter (19.0%), sharing similar peak wind direction frequency with SE winds in spring (NW 15.6% vs. SE 13.4%) and autumn (NW 13.3% vs. SE 11.1%), with this local wind circulation being more frequent in summer (22.2%). The dominance of SE flows in

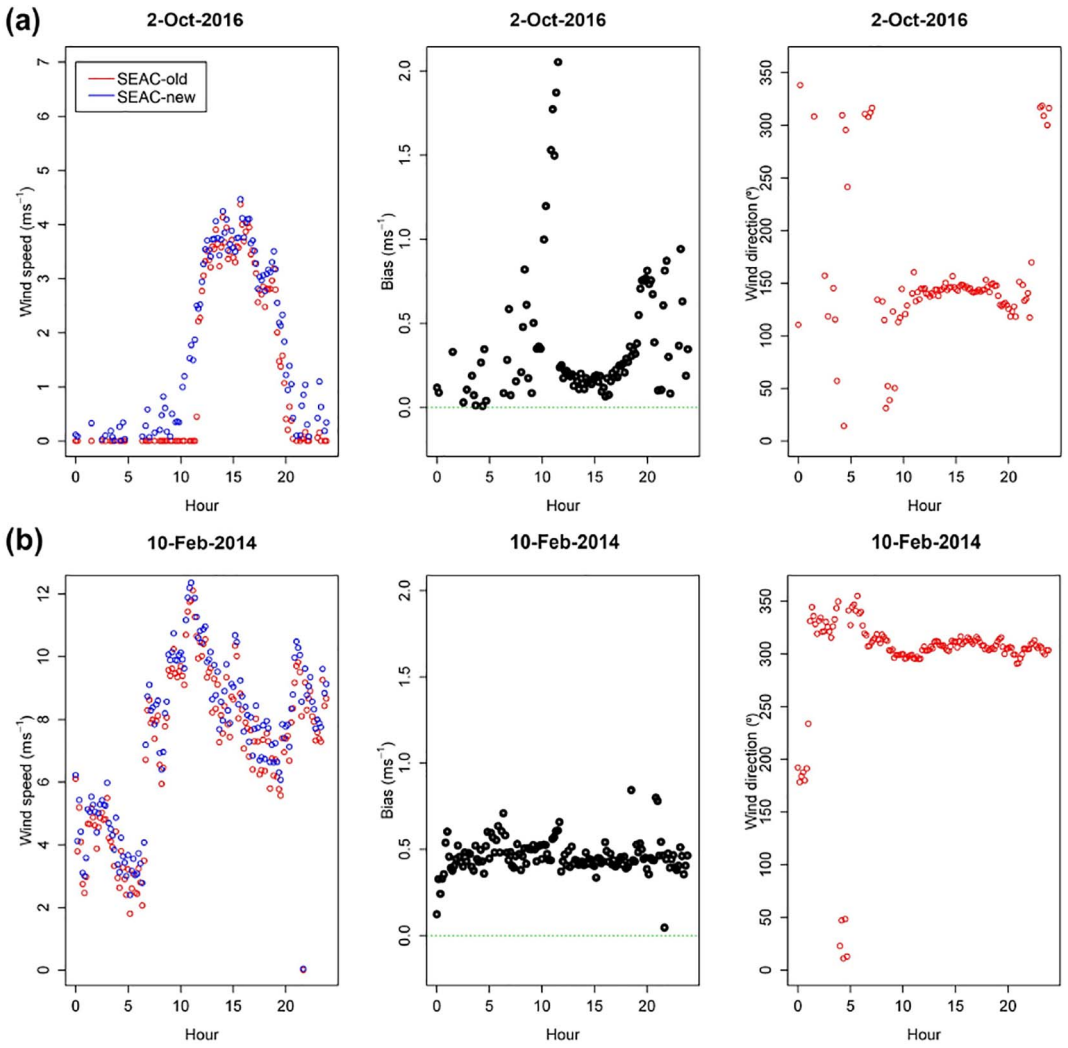

Fig. 4. Wind speed (left) of SEAC-new and SEAC-old, bias (centre) and wind direction (right) on (a) the 2 October 2016 (local SE winds) and (b) the 10 February 2014 (synoptic NW winds). (For interpretation of the references to color in this figure legend, the reader is referred to the web version of this article. The same for the rest of colour figures in the manuscript.)

summer is associated with the development of sea breezes and coastal jets in southeastern Spain (Kottmeier et al. 2000). Monthly, wind roses show a marked cycle in the dominance of these two wind regimes throughout the year. For instance, NW winds dominate from January–April and October–December (peak mean wind speed and wind direction in February with 3.68 m s^{-1} and 27.1%, respectively), and SE flows from May–September (peak mean wind speed in May with 2.28 m s^{-1} and peak wind direction in July with 23.4%). The seasonal-dependent wind regime is suitable for assessing and correcting the anemometer drift under different wind speed intensities and directions throughout the year.

2.4. Statistical modelling

The aim of the statistical modelling proposed is to obtain a robust tool capable of correcting (minimizing) biases in the SEAC-old wind speed series measurements thus obtaining corrected series similar to those measured using SEAC-new. Regression models were used for this purpose as they offer: (i) flexibility to estimate expressions of time; (ii) are able to represent seasonality, non-linear relationships with variables as wind speed; and (iii) capture effects linked to wind direction or other meteorological variables. The regression expression could also allow to interpret the coefficients quantifying the change of bias as a function to the changes in covariate x_j.

First, an exploratory analysis of the bias (i.e., the wind speed difference (in m s^{-1}) between SEAC-new and SEAC-old anemometers at each 10-minute interval) was performed. This exploratory analysis consisted in comparing parallel series and boxplots of the bias distribution at hourly and daily time-steps and covering annual, monthly and seasonal time-scales, following the conventional definition of the four seasons: winter (December–February, DJF), spring (March–May, MAM), summer (June–August, JJA), and autumn (September–November, SON). We applied robust smoothed loess and lowess with time as the predictor variable, since the wind speed and bias distributions are positively skewed and to avoid the effect of outliers (Cleveland, 1979). Second, the Generalized Additive Model (GAM) was used to identify the significant relationship with covariates, which cannot be linear (Hastie and Tibshirani, 1990; Wood, 2017). Third, multiple regression models were proposed and fitted. In the modelling phase, Box-Cox transformation of response is considered and the root square of bias is then selected. The estimation procedure is based in stepwise phase in every of model based in the inclusion of several types of predictor variables. Given previous knowledge, polynomial terms of wind speed of SEAC-old and wind speed data in the previous and next 10-minute periods are used as potential covariates. Furthermore, Fourier harmonics terms based in 24-hour and annual periods are considered to represent possible seasonal behavior. Other indicator variables such as wind direction, calm winds, or periods between sunrise and sunset were used in this statistical modelling. A significance level of $p < 0.01$ and the test of Wald was used to define the simplest

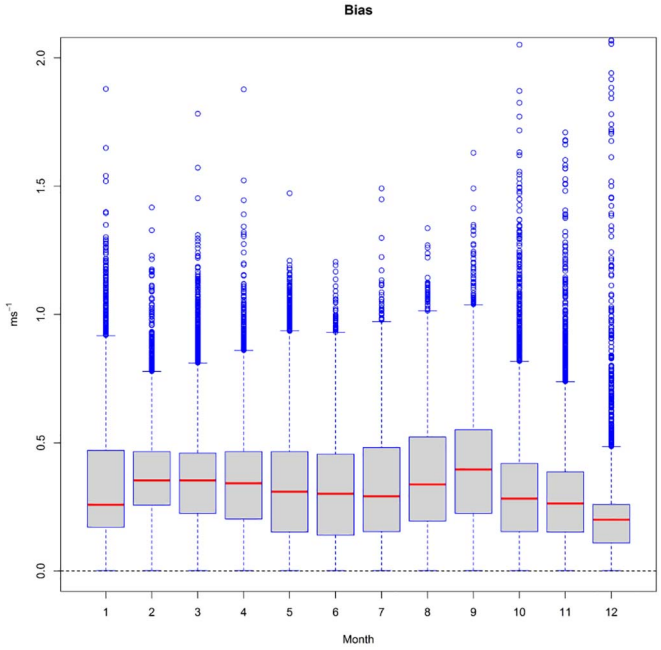

Fig. 5. Box-and-whisker plots of the anemometer bias between SEAC-new and SEAC-old at monthly basis for 2014–2016. The median (red line), the 25th and 75th percentile range (boxes), and the outliers (dots; Y-axis limited up to 2.1 m s^{-1}) are shown. (For interpretation of the references to color in this figure legend, the reader is referred to the web version of this article. The same for the rest of colour figures in the manuscript.)

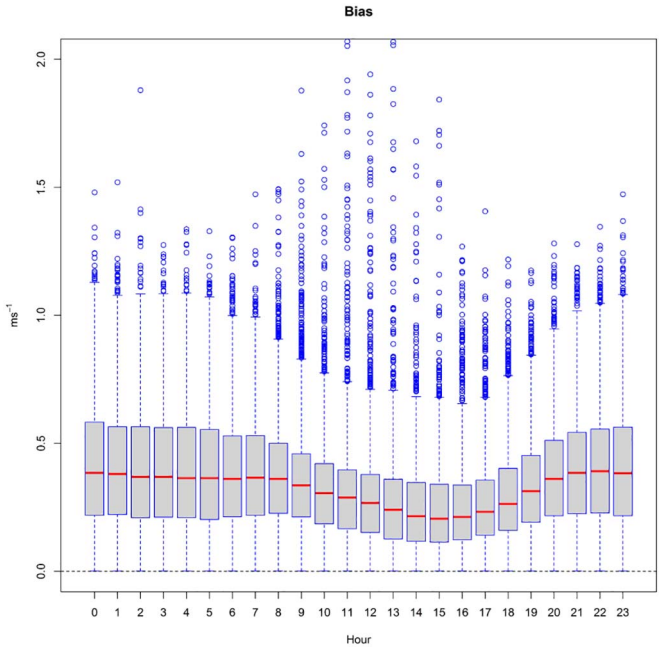

Fig. 6. As Fig. 5, but at an hourly basis. (For interpretation of the references to color in this figure legend, the reader is referred to the web version of this article. The same for the rest of colour figures in the manuscript.)

model, with corrections removing residual autocorrelations (Hyndman and Khandakar, 2008; Abaurrea et al., 2011). Lastly, cross-validation tools were applied to measure the performance of the selected models and heteroscedasticity and normal distribution of residuals are controlled. The R software and VGAM package were used for developing the statistical modelling analyses (Yee et al., 2015).

3. Results

3.1. Case studies of the anemometer bias

Based on the wind climatology shown above, here we present two study cases illustrating main wind regimes in the field experimental site. Fig. 4a shows a representative case study of the daily (at 10-minute intervals) evolution of the wind speed measured by SEAC-new and SEAC-old instruments and the resultant anemometer bias under SE local winds on the 2 October 2016. This is a characteristic example of daylight winds driven by local and sea breeze circulations and nocturnal winds dominated by weak valley or land breeze flows under stable atmospheric conditions. This wind pattern is very common in late-spring (M), summer (JJA) and early autumn (SO) (see Fig. 3), resulting in a variation of the magnitude and different behavior of bias in the transition between night and day in the morning, and between day and night in the evening. For instance, while the SEAC-new anemometer started to rotate at around 06:40 UTC SEAC-old did not register wind until 11:30 UTC. This resulted in a very sharp anemometer bias in the morning of up to 2.05 m s^{-1}. However, a different transition was found in the evening, when wind speed associated with local wind circulations decreased progressively and the SEAC-old ceased earlier than the SEAC-new. In opposition to the sharp bias detected in the morning, the evening transition caused a gradual increase of anemometer bias of up to 0.81 m s^{-1} at around 20:00 UTC. Moreover, a low bias of < 0.20 m s^{-1} occurred around midday hours under unchanging windy conditions (SE sea breeze circulation), whereas some moderate but variable bias of up to 0.94 m s^{-1} lasted from sunset after midnight.

Fig. 4b displays a second case study under moderate to strong large-scale NW synoptic flows on the 10 February 2014, a wind pattern that most likely occur in late autumn (ON), winter (DJF) and early to mid-spring (MA) (see Fig. 3). Under windy conditions lasting the whole day, there is an opposite response of anemometer bias compared to the previous case study, i.e. displaying the same bias magnitude without any sharp breakpoint in bias. Moreover, windy conditions do not lead to large anemometer bias since both SEAC-new and SEAC-old anemometers are rotating at similar rates. However, even under windy conditions biases are not negligible and oscillate around 0.40–0.50 m s^{-1}. This task of analyzing the behavior of anemometer bias served as a basis to define (see Section 4) two regression models to correct (minimize) the weakening effect in wind speed series due to bearing ageing.

3.2. Descriptive statistics of the anemometer bias

Fig. 5 shows box-and-whisker plots of the anemometer bias at monthly basis for the 3-years. There is not a clear monthly cycle in the mean bias between SEAC-new and SEAC-old throughout the year, as shown in Table 2. The minimum mean bias is recorded in December (0.08 m s^{-1}) and the maximum mean bias in February (0.33 m s^{-1}) and September (0.32 m s^{-1}), being mean wind speed differences also high (> 0.2 m s^{-1} on average) for all months, particularly during spring, summer and early autumn. The monthly interquartile range (i.e., first quartile subtracted from the third quartile) in the bias is particularly large (~0.40 m s^{-1}) from May till September (see Fig. 5), denoting a high dispersion of the bias (also exhibited by the standard deviation) from the mean because the dominance of local winds that result in contrasting wind speeds being measured by the two instruments throughout the day (see Fig. 4a). On the contrary, the lower interquartile range is found in December and February (0.22 and 0.26 m s^{-1}, respectively), since large-scale synoptic flows dominate and smaller biases are found between day and night (see Fig. 4b). Extreme biases clearly display an intraannual cycle, with the high maximum bias occurring in autumn and winter months (e.g., February: 3.81 m s^{-1}) and the low maximum bias in spring and summer (e.g., June: 1.20 m s^{-1}).

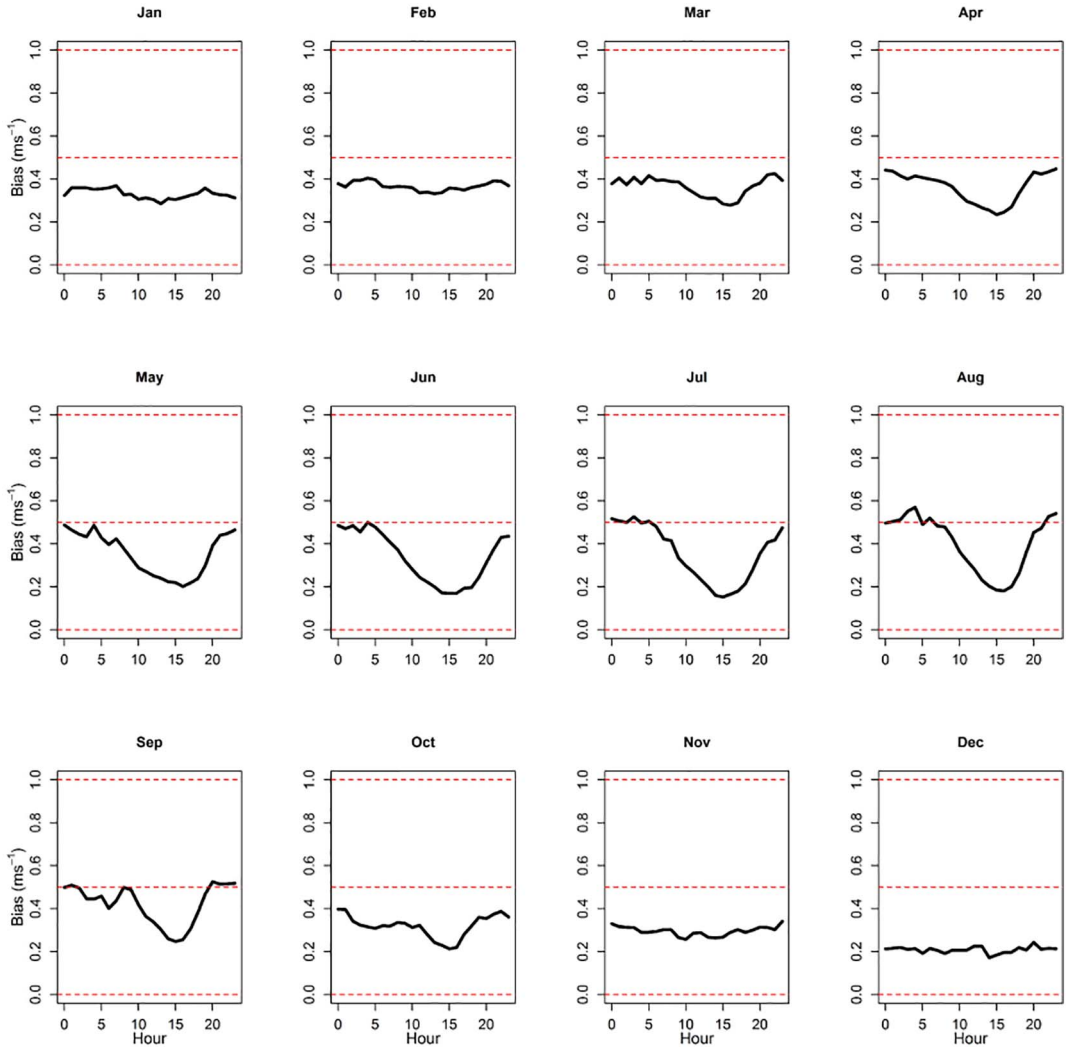

Fig. 7. Hourly mean bias between SEAC-new and SEAC-old at monthly basis for 2014–2016. (For interpretation of the references to color in this figure legend, the reader is referred to the web version of this article. The same for the rest of colour figures in the manuscript.)

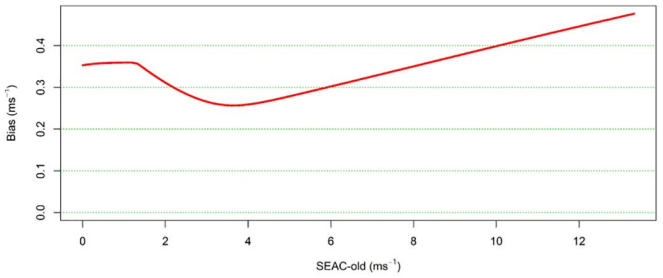

Fig. 8. Anemometer bias between SEAC-new and SEAC-old plotted against wind speed measured by the SEAC-old anemometer for the entire 3-year 2014–2016 period. (For interpretation of the references to color in this figure legend, the reader is referred to the web version of this article. The same for the rest of colour figures in the manuscript.)

At an hourly time-step, Fig. 6 shows a box-and-whisker plot of the anemometer bias by hours. This plot demonstrates a noticeable daily cycle of the anemometer bias, with the low differences occurring during the daylight hours and particularly early in the afternoon (i.e., from 1400 till 1600 h UTC), and the high differences during the whole night (i.e., from 2100 till 8000 h UTC). The interquartile range in the bias also follows a strong daily cycle, being low during the day (e.g., particularly from ~1200 till 1600 h UTC) as both cup anemometers are frequently rotating and wind speed differences tend to be reduced, whereas the bias interquartile range is high at night (e.g., particularly from ~2100 till 0700 h UTC e.g.) since calm or weak winds and much stronger winds can alternate resulting in a dispersion of biases from the mean. Moreover, this box-and-whisker plot also reveals that extreme biases are mostly recorded during daylight hours. More interestingly, even more daily features are revealed when looking at the mean bias at hourly basis for each month as shown in Fig. 7. This plot is very informative about the hourly variations of the mean bias throughout the year, displaying a remarkable monthly pattern. For instance, three phases according to the hourly behavior of the bias are: (i) months with a mean bias that is almost the same during day and night (i.e., ~0.2 and 0.4 m s^{-1}) as shown in January, February, November and December; (ii) months with a strong daily cycle in the mean bias with minimum bias in the afternoon (i.e., ~0.2 and 0.3 m s^{-1}) and maximum bias at night (i.e., ~0.5 and 0.6 m s^{-1}), occurring in May, June, July and August; and (iii) transition months that share mean bias features of these two patterns, with March and October displaying a pattern much more similar to (i), and April and September being more associated with (ii). The different impact of anemometer drift at different timescales, which is crucial for defining a statistical approach for correcting (minimizing) biases in wind speed series, is clearly discernible.

3.3. Anemometer bias as a function of wind speed force

Fig. 8 confirms that temporal patterns of anemometer bias shown above are highly dependent on the wind speed force. A major finding is

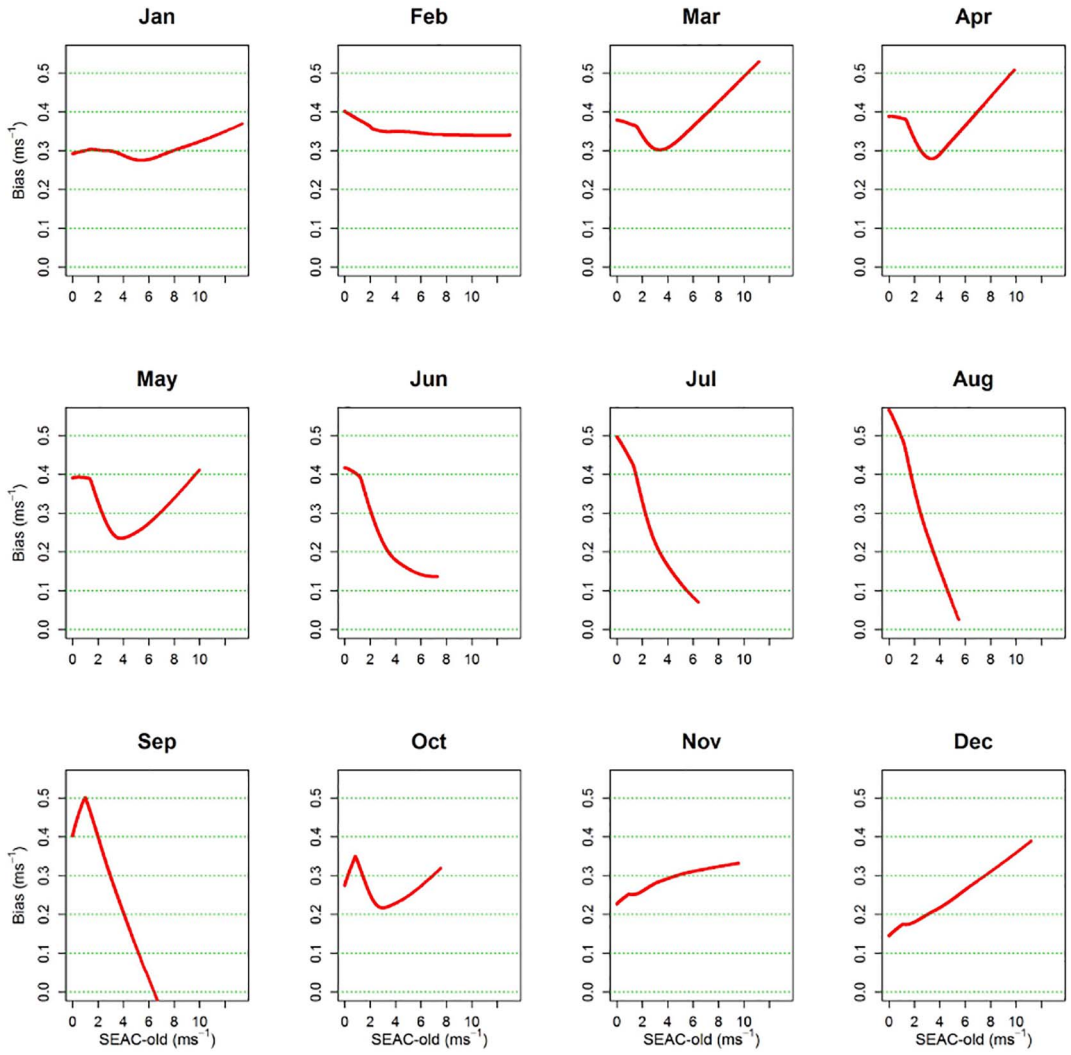

Fig. 9. As Fig. 8, but at monthly basis. (For interpretation of the references to color in this figure legend, the reader is referred to the web version of this article. The same for the rest of colour figures in the manuscript.)

that anemometer biases become larger as wind speed increased, displaying three phases as a function of wind speed force: (i) high biases (around 0.35 m s^{-1}) under weak (< 1.7 m s^{-1}) wind conditions; (ii) a progressive decrease of biases down to around 0.26 m s^{-1} for weak-moderate winds (between 1.8 and 4.0 m s^{-1}); and (iii) a linear increase of biases up to ~0.5 m s^{-1} under moderate to strong winds (above 12 m s^{-1}). However, this pattern strongly varies on a monthly basis (Fig. 9), being quite similar to the described mean annual one in winter, spring and autumn (i.e., January–May and October–December), because the dominance of moderate to strong large-scale synoptic winds, and opposite to this for summer and early autumn (i.e., from June–-September), when no strong winds are observed. For these latter months, the opposite pattern consisted in anemometer biases reaching a marked peak between 0.4 and 0.5 m s^{-1} below winds of 2 m s^{-1}, and progressively decrease down to 0.1 m s^{-1} or even negligible biases above this threshold.

To summarize this finding, annual (Fig. 10) and monthly (Fig. 11) box-and-whisker plots also represent the different response of anemometer biases at different wind speed intervals (Beaufort scale). Annually, the highest median bias corresponds to weak winds (0.3–1.6 m s^{-1} category), whereas the lowest median bias occurs under weak to moderate winds (3.4–5.5 m s^{-1} category). Moreover, the interquartile range in the bias is large for winds < 5.5 m s^{-1}, particularly for the weakest category (0.0–0.3 m s^{-1}), whereas the biases magnitude decreased for moderate to strong winds > 5.5 m s^{-1}. Extreme maximum biases (outliers) mainly occur for the first two categories < 1.6 m s^{-1}, i.e. under very weak wind conditions.

4. A statistical approach to minimize biases

Based on the analysis shown above, two regression models were defined to correct (minimize) biases in wind speed series affected by bearing ageing. Model 1 was formulated using wind speed and temporal terms as covariates; while the Model 2 also added wind direction in its formulation. The main characteristic features used to define regression models are: (i) the non-linear response of the bias, which is also different for almost negligible biases or those that are below the anemometer resolution (i.e., < 0.05 m s^{-1}); (ii) the seasonal and monthly behavior of the bias; (iii) the daily cycle including the sharp bias at the beginning of the day; and (iv) the inertia in the onset and cessation time of anemometers. Table 3 shows the terms defined after conducting the robust exploratory analysis (i.e., Section 3), the proportion of variance explained (R^2 adjusted), and the residual standard deviation for the formulated models that included different covariates.

4.1. Regression Model 1

Model 1 includes as predictor variables for the bias in the time *t* the

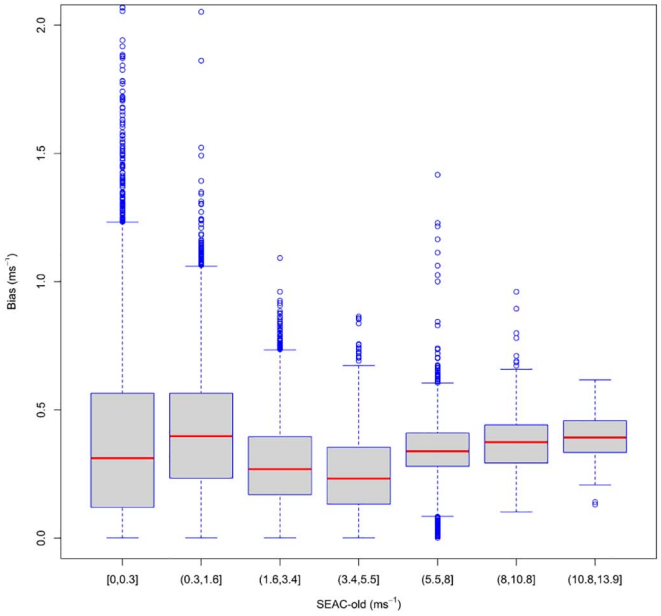

Fig. 10. Box-and-whisker plots of the anemometer bias between SEAC-new and SEAC-old as a function of different wind speed categories (Beaufort scale) from the SEAC-old anemometer for the entire 3-years. The median (red line), the 25th and 75th percentile range (boxes), and the outliers (dots; Y-axis limited up to 2.1 m s^{-1}) are shown. For wind speed ranges in X-axis, square brackets express that limit is included whereas rounded brackets indicate that limit is not included. (For interpretation of the references to color in this figure legend, the reader is referred to the web version of this article. The same for the rest of colour figures in the manuscript.)

term *light*, which indicates if time *t* (at 10-minute intervals) is daylight (i.e., sunrise $< t <$ sunset), and wind speed of SEAC-old at *t*, denoted V_t. Model 1 also incorporates wind speed between *t - 20* to *t + 30* min, applying a parameterization that includes polynomial terms of wind speed of SEAC-old. Additional terms represent the effect of calm, with indicator below the threshold (i.e., < 0.05 m s^{-1}). Fig. 12a shows the fitted biases using Model 1 as a function of the term *Vt* for night and daylight. There is a clear non-linear response of the fitted bias as a function of wind speed at night, whereas the fitted bias is of less magnitude during the daylight hours due to the daily cycle of the anemometer bias (see Section 3.2). Fig. 12b represents the fitted biases using Model 1 as a function of the term $Vt_{+30} - Vt_{-20}$ for non-calm and calm conditions during daylight hours. Under non-calm (i.e., ≥ 0.05) situations, differences in wind speed between $Vt_{+30} - Vt_{-20}$ and biases are low (< 0.3 m s^{-1}) since both anemometers rotate. The opposite occurs under calm conditions at Vt_{-20} and a sharp onset of wind speed at Vt_{+30}, which can lead large biases (> 0.6 m s^{-1}) as the SEAC-new start rotating and the SEAC-old still stopped. Therefore, Model 1 represents the transition from calm to windy conditions in the morning by the term $Vt_{+30} - Vt_{-20}$. As shown in Fig. 10 above, the variability of biases is low for wind speed ranges > 5.5 m s^{-1}, with the percentiles 10 and 90 only differing 0.2 m s^{-1} from the median; this contrasts with the 0.7 m s^{-1} for wind speed ranges < 0.3 m s^{-1}. Therefore, the performance of bias correction differs as a function of wind speed ranges as measured by SEAC-old, as shown in Table 4. The residual standard deviation, calculated as the difference between SEAC-new minus the Model 1 SEAC-old fitted wind speed is lower for moderate to strong wind speed ranges (e.g., 0.114 m s^{-1} for ≥ 8.0 m s^{-1}) than to weak wind speed ranges (e.g., 0.286 m s^{-1} for < 0.3 m s^{-1}). This means that better corrections are achieved by the Model 1 under moderate to strong wind speeds, with this regression model being capable to explain (correct) up to R^2 14.9% of the biases in wind speed series. This percentage of correction increases up R^2 26.7% (see Table 3) when taking into account the harmonic terms which consider the annual, daily and hourly cycles of wind speed. Supplementary Table S1 in Appendix A shows the terms, estimated coefficient and p-value in the Wald test for Model 1.

4.2. Regression Model 2

As defined in Table 4, Model 2 used harmonic terms to describe the temporal cycles of wind speed as the Model 1, and incorporated additional terms based on wind direction. Fig. 13 displays the fitted biases by the Model 2 as a function of the term *Vt*, and stratifying them into 8 wind direction octants. For wind directions ranging from 0° to 180° large bias corrections are applied for weak wind speeds (i.e., < 5.0 m s^{-1}), being reduced them for moderate wind speeds (i.e., 5.0–10 m s^{-1}) and increased again for moderate-strong wind speeds (i.e., > 10.0 m s^{-1}). On the contrary, for wind directions ranging from 180° to 360° large bias corrections are found for moderate-strong wind speeds, reaching fitted values of up to 1.0 m s^{-1}. Moreover, bias corrections are also high for the rest of wind speed ranges, with the fitted biases being particularly constant (and high) for wind directions ranging from 270°–315° and 315°–360°. The combined effect of the wind speed and wind direction in the correction of biases is shown in Fig. 14. The contour plot of fitted biases by Model 2 is different for e.g. SE flows (135°–180°) showing low values (Fig. 14a; except for weak winds) than for NW winds (270°–315°) that display large values (Fig. 14b; particularly under weak and moderate-strong winds). Lastly, the residual standard deviations respond similarly to Model 1, being larger for weak wind speed ranges (e.g., 0.273 m s^{-1} for < 0.3 m s^{-1}) than for moderate wind speeds (e.g., 0.084 m s^{-1} for 3.4–5.5 m s^{-1}) as shown in Table 4. The percentage of explained variance by the Model 2, which includes wind direction, improves the performance of the Model 1 by being capable of correcting up to R^2 37.0%. Supplementary Table S2 in Appendix A shows the terms, estimated coefficient and p-value in the Wald test for Model 2.

4.3. Study cases of wind speed bias corrections

Fig. 15 shows the correction of biases by Model 2 (i.e., the one showing the best correction performance) for two study cases shown previously (Fig. 4). For 2 October 2016 (Fig.15a), dominated by local wind circulations, the corrected SEAC-old wind speed is similar to the SEAC-new wind speed during daylight, with the remaining biases being nearly negligible between ~11:30 UTC till 18:00 UTC. However, the correction of the sharp bias detected at the beginning (or at the end) of the day is not properly adjusted and large biases of up to 1.5 m s^{-1} still remain. For the 10 February 2014 (Fig. 15b), a situation dominated by large-scale synoptic winds, the correction of biases in wind speed series worked more optimally, minimizing biases down to 0 m s^{-1} between ~11:30 UTC till 23:00 UTC, when moderate to strong winds dominate. The bias correction was less optimal during the night, i.e., from ~00:00 UTC till 06:30 UTC, particularly around 05:00 UTC, when weak winds prevailed. It is also worth to mention that Model 2 did not succeed to properly correct a rapid changing bias in wind speed, as that one occurred around 11:00 UTC.

5. Discussion

This experimental study represents a pioneering intercomparison to quantify, and secondarily correct (minimize), anemometer biases due to bearing age in wind speed series. This assessment is particularly novel because of its long-term temporal coverage (i.e., 3-years of 10-minute measurements) conducted at an operational meteorological station as opposed to short-term laboratory experiments (e.g., Vega et al., 2014).

Our results have shown statistically significant ($p < 0.01$) daily (sub-daily) and monthly positive bias in measured mean wind speed between SEAC-new and SEAC-old cup anemometers, confirming that degradation of bearings lead to substantial and temporarily dependent biases. The regression models defined here showed good performance

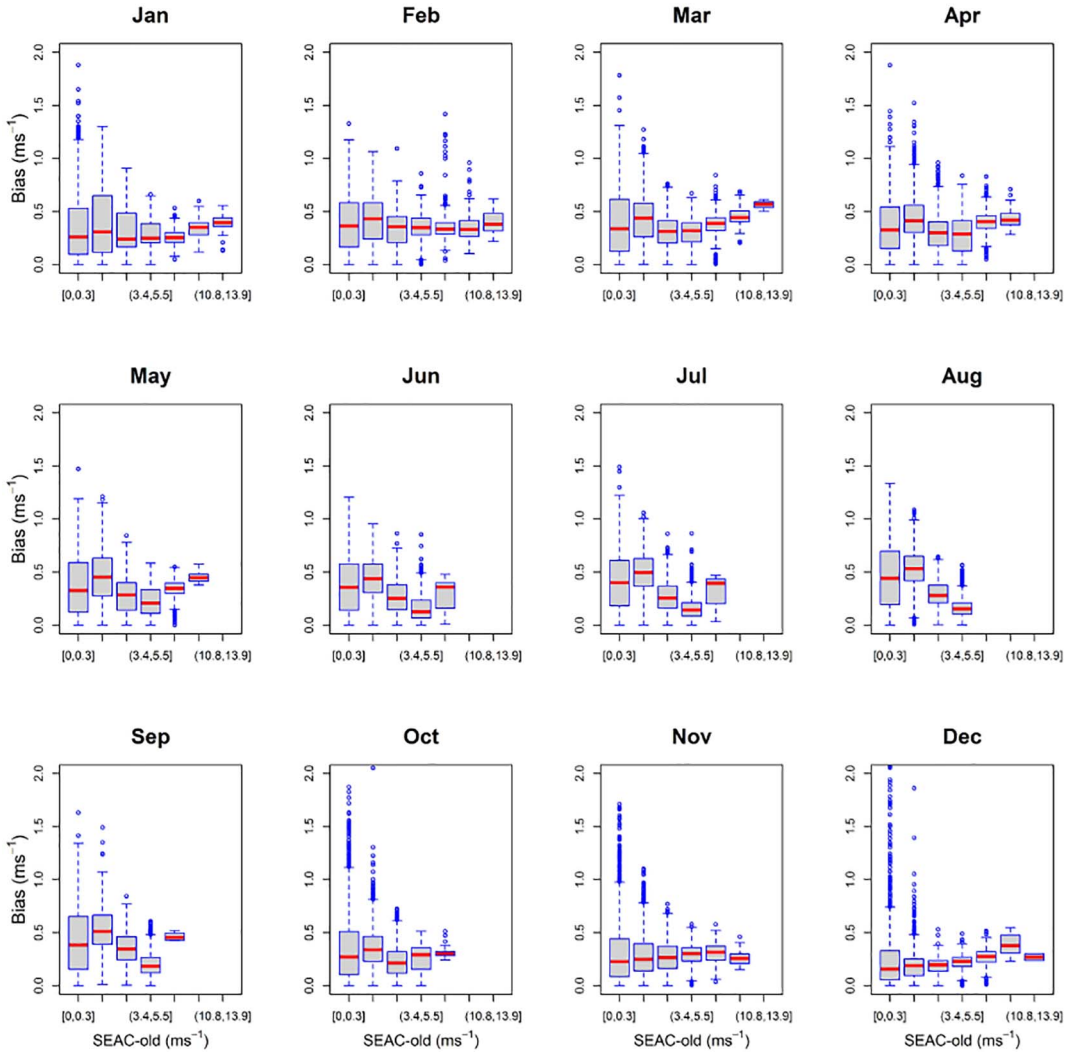

Fig. 11. As Fig. 10, but at a monthly basis. All X-axis data-ranges are labelled on Fig. 10. (For interpretation of the references to color in this figure legend, the reader is referred to the web version of this article. The same for the rest of colour figures in the manuscript.)

Table 3
Proportion (in %) of the explained variance and residual standard deviation by the M1 and M2. The defined terms are associated with wind speed, wind direction, date and hour of the day. Descriptions of the abbreviations for each term are: Y_t = bias at the time t; V_t = wind speed of the SEAC-old at the time t; VUT_t = indicator of V_t under threshold = 0.05 m s^{-1} at the time t;$V_t + d$ = wind speed of the SEAC-old at the time $t + d$; $\Delta V_{t-2,t+3}$ = change of wind speed of the SEAC-old between times $t - 2$ and $t + 3$; *light* = indicator of time between sunrise and sunset; WD_t = wind direccion at the time t.

Model	Predictor	R^2 adj (in %)	Residual standard deviation (in m s^{-1})
M1	V_t, VUT_t	10.7	0.203
	V_{t+d}, VUT_{t+d}, $d = -1,0,1$	11.1	0.203
	light, V_{t+d}, VUT_{t+d}, $d = -2,-1,0,1,2,3$	14.9	0.198
	Harmonic hourly, harmomic daily, light, V_{t+d}, VUT_{t+d}, $d = -2,-1,0,1,2,3$	26.7	0.184
M2	Harm hourly, harm daily, light, V_{t+d}, VUT_{t+d}, $d = -2,-1,0,1,2,3$, WD_t	37.0	0.170

in minimizing the weakening effect in wind speed series due to the bearing ageing, as e.g. Model 2 is able to explain (correct) up to 37.0% of this artificial bias. However, this study is only a statistical approach to characterize and minimize the drifting effect of cup anemometers on wind speed series due to bearing age, and further research is needed to effectively and accurately remove the artificial bias introduced by the degradation of bearings in observed wind speed series for these and other cup anemometers used operational by National Weather Services across the world. This is because instrument errors represent a great challenge and removing anemometer drift signal in historical wind speed series is a very complex task due to multiple issues, e.g. major key constraints are: (i) most long-term wind speed series lack metadata regarding replacements of anemometers and of in-situ and periodical inspections or recalibrations to ensure the quality of wind speed measurements (Azorin-Molina et al., 2014), which introduces a challenge of knowing when applying corrections in the series should be applied; (ii) our field experiment was conducted using the most common cup anemometer device (i.e., SEAC SV5) used by the Spanish AEMET in the AWS since the mid-1980s, which limits the application of our correction model to wind speed series recorded with different anemometer devices that may have different response to bearing ageing; (iii) even employing the same anemometer device (e.g., the SEAC SV5 in Spain), anemometer ageing rates vary depending on the environmental and climate conditions at each location since (the same for other climate variables such as air temperature; Brunet et al., 2011) e.g. the degradation of bearings might be very sensitive to some places more windy or dusty (or salt nuclei) than others; (iv) the gradual drift of bearing malfunction on historical wind speed series is not detected as a sharp breakpoint (e.g., as due to anemometer replacement,

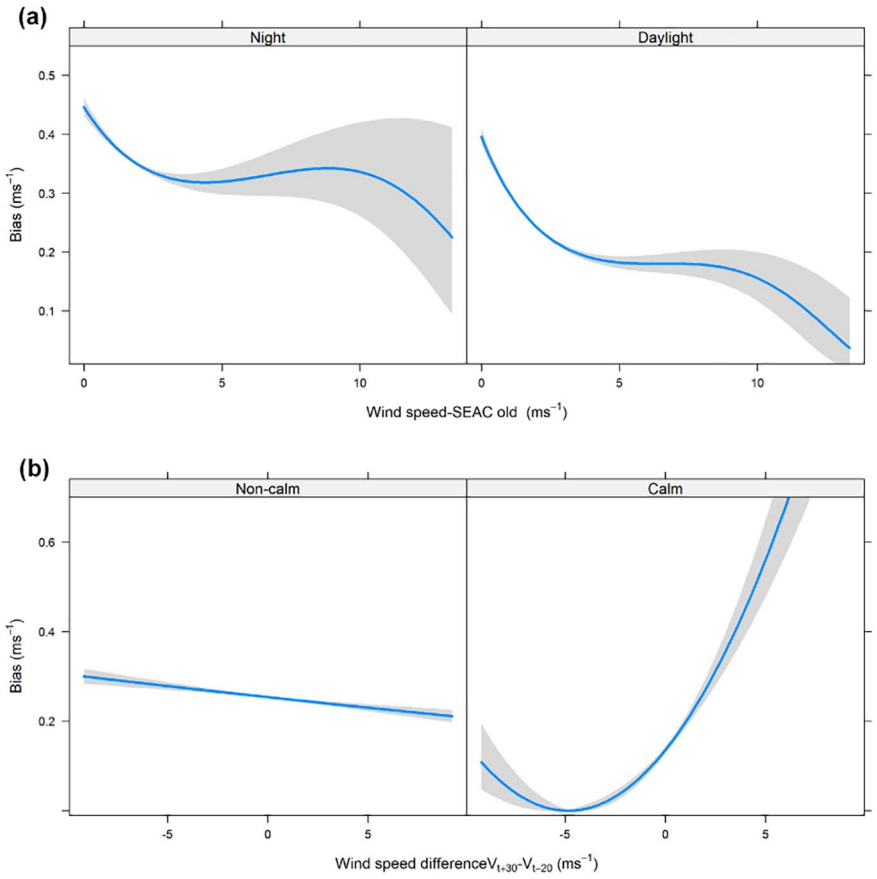

Fig. 12. (a) Fitted bias by the Model 1 as a function of wind speed of the SEAC-old (Vt) during night (left) and daylight (right). The rest of predictors remain in its mean value. Shaded grey over the fitted line represents the 95% confidence band for the fitted value. (b) The same as (a) but as a function of the difference in wind speed for a temporal window from Vt_{-20} and Vt_{+30} min for non-calm (left) and calm (right) situations during daylight hours. (For interpretation of the references to color in this figure legend, the reader is referred to the web version of this article. The same for the rest of colour figures in the manuscript.)

Table 4
R^2 adjusted and residual standard deviation of the Model 1 and Model 2, for the different wind speed ranges defined by the Beaufort scale. For wind speed ranges, square brackets express that limit is included whereas rounded brackets indicate that limit is not included.

		Residual standard deviation (in m s^{-1})					
Model	R^2 adj (in %)	V_t < 0.3 m s^{-1}	V_t in [0.3, 1.6]	V_t in [1.6, 3.4]	V_t in [3.4, 5.5]	V_t in [5.5, 8]	V_t ≥ 8 m s^{-1}
M1	14.9	0.286	0.215	0.147	0.133	0.129	0.114
M2	37.0	0.273	0.186	0.119	0.084	0.107	0.107

anemometer height change), which means that biases increase progressively and imperceptibly over the time; and (v) the degradation of cup anemometers due to wear and tear may not only be due to bearing malfunctions, yet also to the mass addition of dirt to cups, which has not been quantified here or previously.

These key constraints reveal the major limitations for a comprehensive assessment and minimization of anemometer drift in wind speed series, and highlight new areas of improvement. First, in the absence of metadata, there is a need in most National Weather Services across the world to rescue technical notes regarding e.g. relocation of stations, type of anemometers, anemometer height changes, instrument malfunctions, etc., which is actually stored in notebooks (i.e., in non-digital form), define a protocol for official weather observers to compile this information at each meteorological station, and make such metadata available for users (Aguilar et al., 2003). Second, a field experimental design comparing the most common anemometer devices (new vs. old and different manufacturing) other than the SEAC SV5 and used by National Weather Services across the world is also needed, an initiative that will need help from e.g. the Commission for Instruments and Methods of Observation (CIMO; http://www.wmo.int/pages/prog/www/CIMO/AboutCIMO.html; last accessed 1 November 2017) of the World Meteorological Organization. Third, and last, this initiative should be implemented in different environmental and climate conditions, and in addition to assessing anemometer drift due to bearing malfunctions should also include the degradation due to dirt in the cups. Future experiments should be conducted at best quality meteorological stations where dust and air quality data are recorded. Recently, parallel wind speed comparisons of standard universal anemographs and Vaisala sensors were conducted by Brázdil et al. (2017) in the Czech Republic to quantify the impact of changes in the anemometer type in the stilling phenomenon. They found that Vaisala sensors measure higher wind speed than universal anemographs, particularly in calm situations and at low wind speeds.

Despite the abovementioned constraints and future work, our field experimental study represents the first long-term, field-based, robust assessment and minimization of the impact of anemometer drift, which has been hypothesized as a partial cause of stilling. The regression models defined showed usefulness in minimizing biases, with Model 1 having potential to be applied to other sites as it is only based on wind speed terms, and Model 2 showing its strength when combining wind speed with wind direction terms. However, further work is needed to fill the niche of the application of our correction methodology to other stations and wind speed series; this is a next logical step in our research. Moreover, for a complete correction of biases, the regression model would be a first adjustment followed by the application of a quality control and homogenization protocol as those defined by e.g. Wan et al. (2010), Azorin-Molina et al. (2014, 2016), Minola et al. (2016). Sonic anemometers can strongly avoid biases in wind speed series due to anemometer drift since they: (i) do not require scheduled maintenance (e.g., re-oiling bearing) as being designed with no moving parts; (ii) are accurate at low wind speeds (measurement threshold of 0.0 m s^{-1})

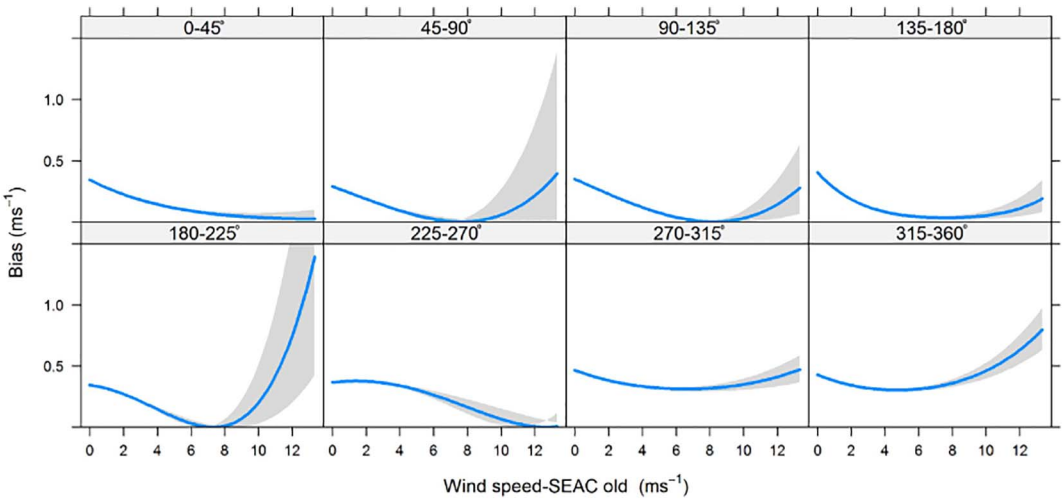

Fig. 13. Fitted bias by the Model 2 as a function of wind speed of the SEAC-old (V_t) and stratified by 8 wind direction octants (in degrees). The rest of predictors remain in its mean value. Shaded grey over the fitted line represents the 95% confidence band for the fitted value. (For interpretation of the references to color in this figure legend, the reader is referred to the web version of this article. The same for the rest of colour figures in the manuscript.)

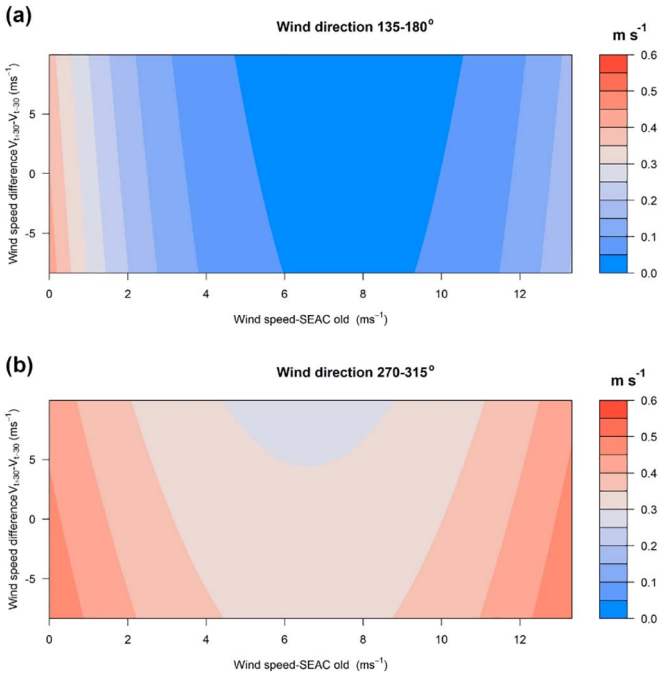

Fig. 14. Contour plot of the fitted bias by Model 2 as a function of wind speed of the SEAC-old (Vt) and the difference in wind speed for a temporal window from $Vt - 30$ and $Vt + 30$ min under (a) SE flows (135°–180°), and (b) NW winds (270°-315°). The rest of predictors remain in its mean value. (For interpretation of the references to color in this figure legend, the reader is referred to the web version of this article. The same for the rest of colour figures in the manuscript.)

compared to cup anemometers that because of friction have a higher measurement threshold; and (iii) do not need calibration because wind velocity is measured using ultrasonic sound waves (Cueva and Sanz-Andres, 2000). However, the simplicity and low price of cup anemometers compared to sonic or propeller devices means that numerous National Weather Services, and the wind-energy industry, are still using this instrument. Therefore, wind speed series are biased by anemometer drift and further efforts to minimize errors are needed. Among them, to effectively and accurately assessing the performance of degradation of bearings and anomaly detection, Pindado et al. (2014) suggest to apply Fourier analysis sampling the voltage output of cup anemometers during e.g. 20 s as proposed Vega et al. (2014). Moreover, the introduction of new terms (e.g., other atmospheric parameters) in the definition of the regression models could hytothetically increase the percentage of bias correction. Finally, to conclude, our approach contributes to the state-of-the-art of quality control and homogenization techniques to minimize errors in wind speed series aimed at better assessing long-term trends and variability from high-quality and homogeneous wind records.

6. Conclusion

The major findings of this 3-year intercomparison study using the same cup anemometer with new vs. old bearings are:

(i) Statistically significant daily (sub-daily) and monthly positive biases in measured mean wind speed between SEAC-new and SEAC-old anemometers were detected; confirming that degradation of bearings lead to substantial and temporarily dependent biases. Large biases were mainly detected under weak or strong winds. The stronger the wind, the larger the bias.

(ii) The two regression models developed here had a reasonable performance in mimicking the weakening effect in wind speed series due to the bearing ageing. The Model 2 that includes information about the time of the day (i.e., representing some possible daily cycle) and wind direction as independent variables is able to explain (correct) up to 37% of this artificial bias. This highlights the importance of proper calibration of the old instruments.

(iii) Further research is needed to develop methods to more effectively and precisely remove biases due to instrumental artefacts in observed wind speed series. Particularly new field experimental designs using a wide range of manufactured cup anemometers (e.g., those used by key National Weather Services) and ages, under contrasting climatic conditions would be helpful to establish correction methods for different instruments with different ages.

Acknowledgements

C. A-M. has received funding from the European Union's Horizon 2020 research and innovation programme under the Marie Skłodowska-Curie grant agreement No. 703733 (STILLING project). This research was supported by the research projects: Swedish BECC, MERGE, VR (2014-5320), and, partially, from the research group “Modelos Estocásticos” supported by Aragon Government and the European Social Fund. We particularly thanks Isidoro Sojo and Alfredo Avia from

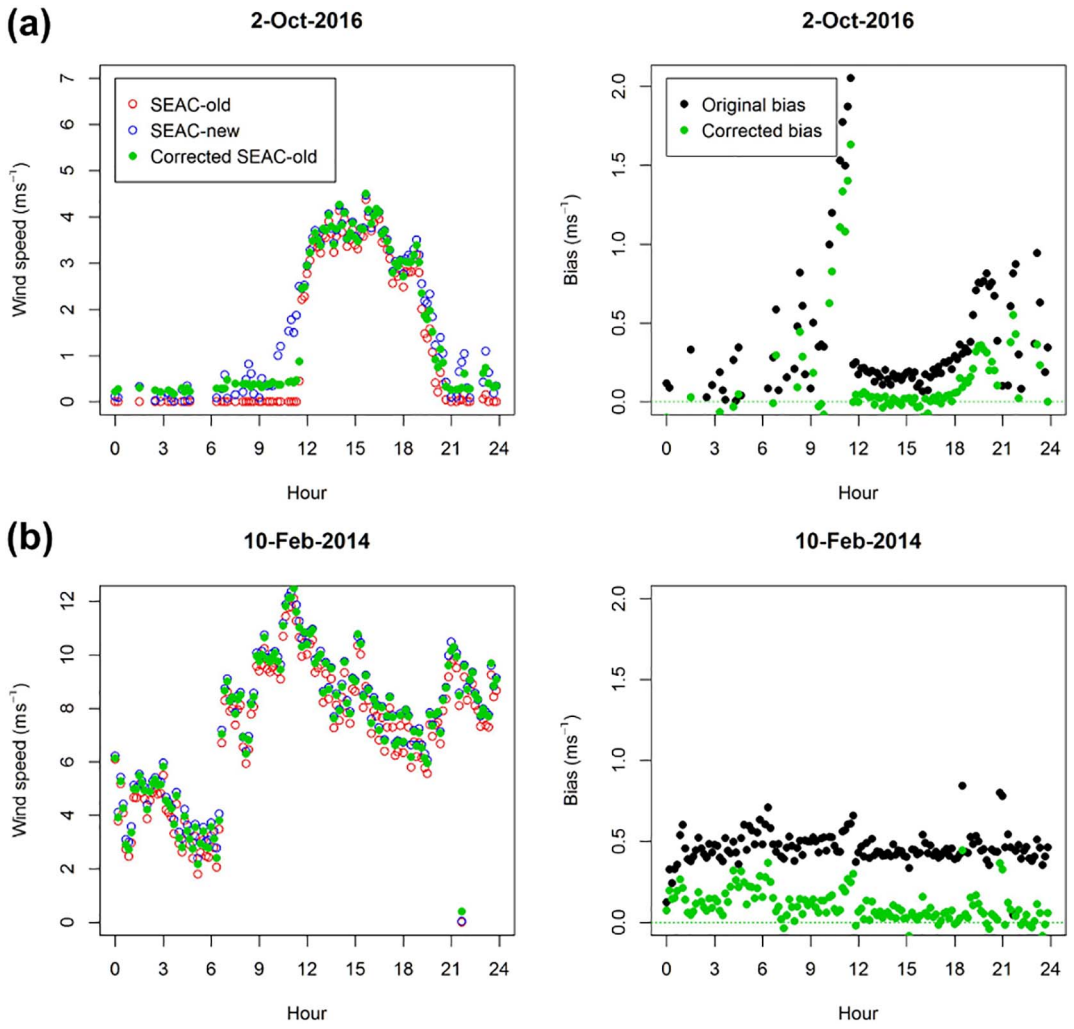

Fig. 15. Hourly wind speed of SEAC-new, SEAC-old and corrected SEAC-old (left graphs), and original and corrected bias (right graphs), on (a) the 2 October 2016 (local SE winds) and (b) the 10 February 2014 (synoptic NW winds). The bias corrections are applied using Model 2. (For interpretation of the references to color in this figure legend, the reader is referred to the web version of this article. The same for the rest of colour figures in the manuscript.)

SEAC for their help on the maintenance of the SEAC-old and the wind tunnel tests performed. The authors wish to acknowledge the anonymous reviewers for their detailed and helpful comments to the original manuscript.

Appendix A. Supplementary data

Supplementary data to this article can be found online at https://doi.org/10.1016/j.atmosres.2017.12.010.

References

Abaurrea, J., Asin, J., Cebrian, A.C., Garcia-Vera, M.A., 2011. Trend analysis of water quality series based on regression models with correlated errors. J. Hydrol. 400 (3), 341–352. http://dx.doi.org/10.1016/j.jhydrol.2011.01.049.

Aguilar, E., Auer, I., Brunet, M., Peterson, T.C., Wieringa, J., 2003. Guidelines on climate metadata and homogenization. World Meteorol. Organ. 1186, 1–52. Available online at. http://www.wmo.int/datastat/documents/WCDMP-53_1.pdf, Accessed date: 11 January 2017.

Azorin-Molina, C., Martin-Vide, J., 2007. Methodological approach to the study of the daily persistence of the sea breeze in Alicante (Spain). Atmosfera 20 (1), 57–80.

Azorin-Molina, C., Tijm, S., Chen, D., Baldi, M., 2011. A multi-year study of sea breezes in a Mediterranean coastal site: Alicante (Spain). Int. J. Climatol. 31 (3), 468–486. http://dx.doi.org/10.1002/joc.2064.

Azorin-Molina, C., Vicente-Serrano, S.M., McVicar, T.R., Jerez, S., Sanchez-Lorenzo, A., López-Moreno, J.I., Revuelto, J., Trigo, R.M., Lopez-Bustins, J.A., Espirito-Santo, F., 2014. Homogenization and assessment of observed near-surface wind speed trends over Spain and Portugal, 1961–2011. J. Clim. 27 (10), 3692–3712. http://dx.doi.org/10.1175/JCLI-D-13-00652.1.

Azorin-Molina, C., Guijarro, J.A., McVicar, T.R., Vicente-Serrano, S.M., Chen, D., Jerez, S., Espírito-Santo, F., 2016. Trends of daily peak wind gusts in Spain and Portugal, 1961–2014. J. Geophys. Res. - Atmos. 121 (3), 1059–1078. http://dx.doi.org/10.1002/2015JD024485.

Azorin-Molina, C., Vicente-Serrano, S.M., McVicar, T.R., Revuelto, J., Jerez, S., Lopez-Moreno, J.I., 2017a. Assessing the impact of measurement time interval when calculating wind speed means and trends under the stilling phenomenon. Int. J. Climatol. 37 (1), 480–492. http://dx.doi.org/10.1002/joc.4720.

Azorin-Molina, C., Dunn, R.J.H., Mears, C.A., Berrisford, P., McVicar, T.R., 2017b. [Global climate; atmospheric circulation] surface winds [in "state of the climate in 2016"]. Bull. Amer. Meteor. Soc. 98 (8), S37–S39. http://dx.doi.org/10.1175/2017BAMSStateoftheClimate.

Bichet, A., Wild, M., Folini, D., Schär, C., 2012. Causes for decadal variations of wind speed over land: sensitivity studies with a global climate model. Geophys. Res. Lett. 39 (11), L11701. http://dx.doi.org/10.1029/2012GL051685.

Brázdil, R., Valík, A., Zahradníček, P., Řezníčková, L., Tolasz, R., Možný, M., 2017. Windstilling in the light of wind speed measurements: the Czech experience. Clim. Res. http://dx.doi.org/10.3354/cr01492. (in press).

Brunet, M., Asin, J., Sigro, J., Bañón, M., García, F., Aguilar, E., Palenzuela, J.E., Peterson, T.C., Jones, P., 2011. The minimization of the screen bias from ancient Western Mediterranean air temperatura records: an exploratory statistical analysis. Int. J. Climatol. 31 (12), 1879–1895. http://dx.doi.org/10.1002/joc.2192.

Charnock, H., Pierce, F.E., 1959. New housing for the sensitive cup-contact anemometer, Mk. 1. J. Sci. Instrum. 37 (7), 329. http://dx.doi.org/10.1088/0950-7671/36/7/124.

Cleveland, W.S., 1979. Robust locally weighted regression and smoothing scatterplots. J. Am. Stat. Assoc. 74 (368), 829–836. http://dx.doi.org/10.2307/2286407.

Cueva, A., Sanz-Andres, A., 2000. On sonic anemometer measurement theory. J. Wind Eng. Ind. Aerodyn. 88 (1), 25–55. http://dx.doi.org/10.1016/S0167-6105(00)00023-4.

Deacon, E.L., 1951. The over-estimation error of cup anemometers in fluctuating winds. J. Sci. Instrum. 28, 231–234.

Dunn, R.J.H., Azorin-Molina, C., Mears, C.A., Berrisford, P., McVicar, T.R., 2016. [Global climate; atmospheric circulation] surface winds [in "state of the climate in 2015"]. Bull. Amer. Meteor. Soc. 97 (8), S38–S40. http://dx.doi.org/10.1175/2016BAMSStateoftheClimate.1.

Hastie, T., Tibshirani, R., 1990. Generalized Additive Models. Chapman & Hall, London.

Hyndman, R.J., Khandakar, Y., 2008. Automatic time series forecasting: the forecast Package for R. J. Stat. Softw. 27 (3), 1–22. http://dx.doi.org/10.18637/jss.v027.i03.

Jacobson, M.Z., Kaufman, Y.J., 2006. Wind reduction by aerosol particles. Geophys. Res. Lett. 33 (24), L24814. http://dx.doi.org/10.1029/2006GL027838.

Kim, J., Paik, K., 2015. Recent recovery of surface wind speed after decadal decrease: a focus on South Korea. Clym. Dyn. 45 (5), 1699–1712. http://dx.doi.org/10.1007/s00382-015-2546-9.

Kimura, S., Abe, K., Tsuboi, K., Tammelin, B., Suzuki, K., 2001. Aerodynamic characteristics of an iced cup-shaped body. Cold Reg. Sci. Technol. 33 (1), 45–58. http://dx.doi.org/10.1016/S0165-232X(01)00026-X.

Kottmeier, C., Palacio-Sese, P., Kalthoff, N., Corsmeier, U., Fiedler, F., 2000. Sea breezes and coastal jets in southeastern Spain. Int. J. Climatol. 20 (14), 1791–1808. http://dx.doi.org/10.1002/1097-0088.

Kristensen, L., 1998. Cup anemometer behavior in turbulent environments. J. Atmos. Ocean. Technol. 15 (1), 5–17. http://dx.doi.org/10.1175/1520-0426(1998)015<0005:CABITE>2.0.CO;2.

Limjirakan, S., Limsakul, A., 2012. Trends in Thailand pan evaporation from 1970 to 2007. Atmos. Res. 108, 122–127. http://dx.doi.org/10.1016/j.atmosres.2012.01.010.

Lu, J., Vecchi, G.A., Reichler, T., 2007. Expansion of the Hadley cell under global warning. Geophys. Res. Lett. 34 (6), L06805. http://dx.doi.org/10.1029/2006GL028443.

Makkonen, L., Lehtonen, P., Helle, L., 2001. Anemometry in icing conditions. J. Atmos. Ocean. Technol. 18 (9), 1457–1469. http://dx.doi.org/10.1175/1520-0426(2001)018<1457:AIIC>2.0.CO;2.

Martinez, A., Vega, A., Pindado, S., Meseguer, E., García, L., 2016. Deviations of cup anemometer rotational speed measurements due to steady state harmonic accelerations of the rotor. Measurement 90, 483–490. http://dx.doi.org/10.1016/j.measurement.2016.05.011.

Marvin, C.F., 1932. A rational theory of the cup anemometer. Mon. Weather Rev. 60 (2), 43–56. http://dx.doi.org/10.1175/1520-0493(1932)60<43:ARTOTC>2.0.CO;2.

Marvin, C.F., 1934. Recent advances in anemometry. Mon. Weather Rev. 62 (4), 115–120. http://dx.doi.org/10.1175/1520-0493(1934)62<115:RAIA>2.0.CO;2.

Mazzarella, A., 2007. The 60-year solar modulation of global air temperature: the Earth's rotation and atmospheric circulation connection. Theor. Appl. Climatol. 88 (3–4), 193–199. http://dx.doi.org/10.1007/s00704-005-0219-z.

McVicar, T.R., Roderick, M.L., Donohue, R.J., Li, L.T., Van Niel, T.G., Thomas, A., Grieser, J., Jhajharia, D., Himri, Y., Mahowald, N.M., Mescherskaya, A.V., Kruger, A.C., Rehman, S., Dinpashoh, Y., 2012. Global review and synthesis of trends in observed terrestrial near-surface wind speeds: implications for evaporation. J. Hydrol. 416–417, 182–205. http://dx.doi.org/10.1016/j.jhydrol.2011.10.024.

Minola, L., Azorin-Molina, C., Chen, D., 2016. Homogenization and assessment of observed near-surface wind speed trends across Sweden, 1956–2013. J. Clim. 29 (20), 7397–7415. http://dx.doi.org/10.1175/JCLI-D-15-0636.1.

Patterson, J., 1926. The cup anemometer. Trans. R. Soc. Can. Ser. III 20, 1–54.

Pindado, S., Barrero-Gil, A., Sanz, A., 2012. Cup anemometers' loss of performance due to ageing processes, and its effect on annual energy production (AEP) estimates. Energies 5 (5), 1664–1685. http://dx.doi.org/10.3390/en5051664.

Pindado, S., Cubas, J., Sorribes-Palmer, F., 2014. The cup anemometer, a fundamental meteorological instrument for the wind energy industry. Research at the IDR/UPM Institute. Sensors 14 (11), 21418–21452. http://dx.doi.org/10.3390/s141121418.

Pindado, S., Cubas, J., Sorribes-Palmer, F., 2015. On the harmonic analysis of cup anemometer rotation speed: a principle to monitor performance and maintenance status of rotating meteorological sensors. Measurement 73, 401–418. http://dx.doi.org/10.1016/j.measurement.2015.05.032.

Robinson, T.R., 1847–1850. On a new anemometer. Proc. R. Irish Acad. 1836–1869 (4), 566–572.

Roderick, M.L., Rotstayn, L.D., Farquhar, G.D., Hobbins, M.T., 2007. On the attribution of changing pan evaporation. Geophys. Res. Lett. 34 (17), L17403. http://dx.doi.org/10.1029/2007GL031166.

Shuttleworth, W.J., Serrat-Capdevilla, A., Roderick, M.L., Scott, R.L., 2009. On the theory relating changes in area-average and pan evaporation. Quart. J. Roy. Meteorol. Soc. 135 (642), 1230–1247. http://dx.doi.org/10.1002/qj.434.

Siegel, D., Lee, J., 2011. An auto-associative residual processing and K-means clustering approach for anemometer health assessment. Int. J. Progn. Health Manag. 14 (2), 1–12.

Sun, L., Chen, C., Cheng, Q., 2012. Feature extraction and pattern identification for anemometer condition diagnosis. Int. J. Progn. Health Manag. 3 (1), 1–11.

Tong, L., Zhang, H., Yu, J., He, M., Xu, N., Zhang, J., Qian, F., Feng, J., Xiao, H., 2017. Characteristics of surface ozone and nitrogen oxides at urban, suburban and rural sites in Ningbo, China. Atmos. Res. 187, 57–68. http://dx.doi.org/10.1016/j.atmosres.2016.12.006.

Vautard, R., Cattiaux, J., Yiou, P., Thépaut, J.-N., Ciais, P., 2010. Northern hemisphere atmospheric stilling partly attributed to an increase in surface roughness. Nat. Geosci. 3 (11), 756–761. http://dx.doi.org/10.1038/ngeo979.

Vega, E., Pindado, S., Martínez, A., Meseguer, E., Garcia, L., 2014. Anomaly detection on cup anemometers. Meas. Sci. Technol. 25 (12), 127002. http://dx.doi.org/10.1088/0957-0233/25/12/127002.

Wan, H., Xiaolan, L.W., Swail, V.R., 2010. Homogenization and trend analysis of Canadian near-surface wind speeds. J. Clim. 23 (5), 1209–1225. http://dx.doi.org/10.1175/2009JCLI3200.1.

Wever, N., 2012. Quantifying trends in surface roughness and the effect on surface wind speed observations. J. Geophys. Res. - Atmos. 117 (D11), D11104. http://dx.doi.org/10.1029/2011JD017118.

WMO, 2008. WMO guide to meteorological instruments and methods of observation. In: World Meteorological Organization. WMO, Geneva, Switzerland No. 8.

Wood, S.N., 2017. Generalized Additive Models: An Introduction with R. Chapman and Hall/CRC (476 pp).

Xu, M., Chang, C.P., Fu, C., Qi, Y., Robock, A., Robinson, D., Zhang, H., 2006. Steady decline of East Asian monsoon winds, 1969–2000: evidence from direct ground measurements of wind speed. J. Geophys. Res. - Atmos. 111 (D24), D24111. http://dx.doi.org/10.1029/2006JD007337.

Yee, T.W., Stoklosa, J., Huggins, R.M., 2015. The VGAM package for capture–recapture data using the conditional likelihood. J. Stat. Soft. 65 (5), 1–33. http://dx.doi.org/10.18637/jss.v065.i05.